SUPPLEMENTARY MATERIAL

Steady dynein forces induce flutter instability and propagating waves in mathematical models of flagella

PV Bayly and SK Dutcher

SUPPLEMENTARY MATERIAL - APPENDICES

A. DERIVATION OF EQUATIONS OF MOTION

The equations of motion of two coupled doublets are derived below. This derivation follows reference (1) which in turn is based on the flagella model of Hines and Blum (2). Each doublet is modeled as a slender elastic beam in viscous fluid, subject to both active and passive inter-doublet forces

A.1 Equilibrium conditions, kinematics, and constitutive relationships

The equilibrium equations are written in terms of the two tangent angles ψ_1 and ψ_2, the net internal tangential and normal force components in each doublet (T_1, N_1, T_2, N_2), and the external viscous force components per unit length (q_T and q_N). The baseline separation between doublets in this model is the effective diameter, a. The net inter-doublet shear (tangential) force component, f_T, is due to distributed active (dynein arms) and passive elements (nexin links, e.g.). In addition, these elements also provide a transverse inter-doublet force component, f_N.

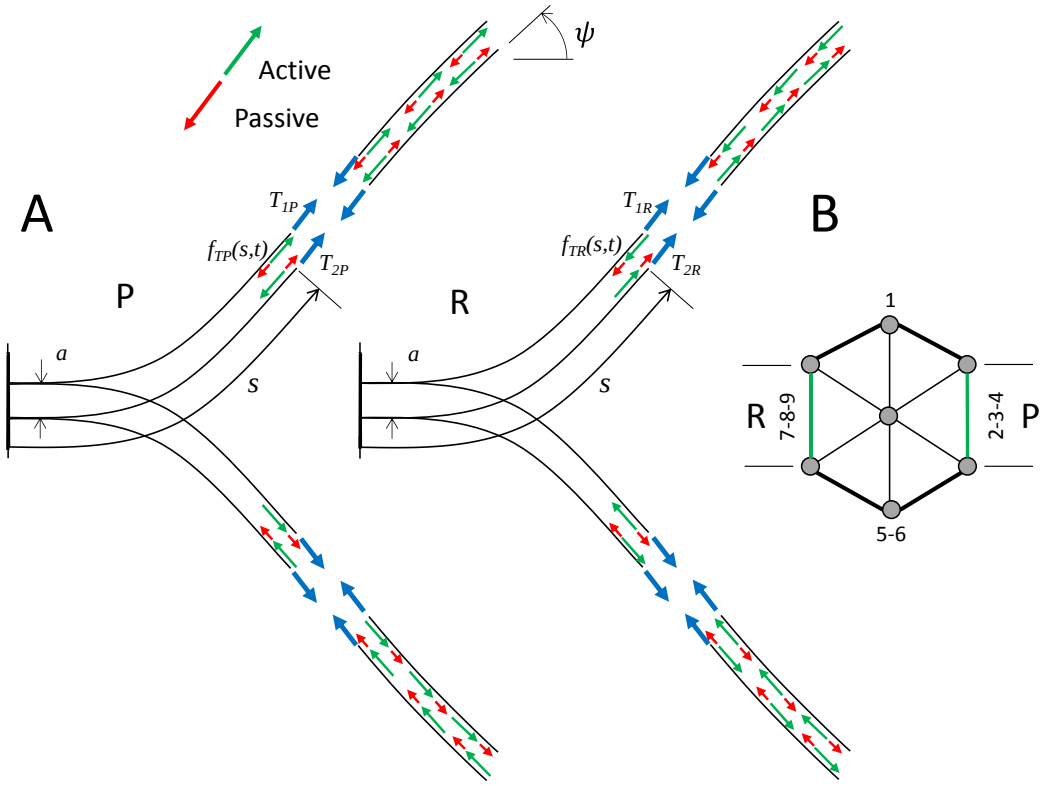

Supplementary Figure S1. The current models are based on two pairs of doublets driving flagellar bending. (**A**) Side views of P and R doublet pairs show sliding displacement, effective diameter a, active (green) and passive (red) shear forces ($f_{TP}(s,t)$ and $f_{TR}(s,t)$) and internal doublet tension (T_{1P}, T_{2P}, T_{1R}, T_{2R}). (**B**) Representation of the axoneme by a simplified structural model with six doublets, of which two pairs are active. Activity on the P side drives doublet 4 tip-ward relative to doublet 2; R activity drives doublet 9 tip-ward relative to doublet 7. Reproduced from reference (1). The moment per unit length produced by inter-doublet components is: $m = \frac{a}{2}(f_{TP} - f_{TR})$ (1). If active shear forces are equal on P and R sides, a straight equilibrium position will exist with tension and compression in the active doublets (see **Fig. 3**).

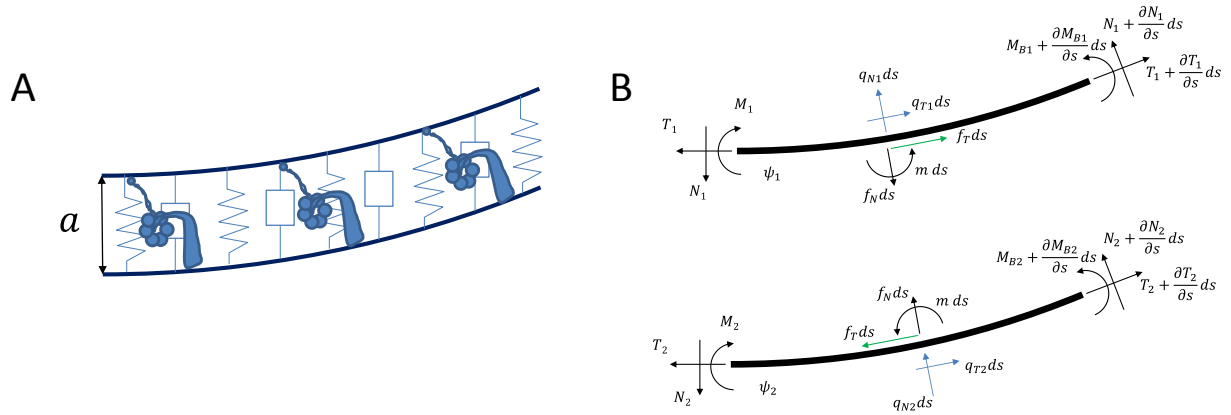

Supplementary Figure S2. (**A**) Schematic representation of inter-doublet mechanics, consisting of active dynein arms and passive elastic and viscous components. (**B**) Free-body diagram of a differential element of the two-doublet model of the axoneme. See also **Fig. S1**, and **Fig. 3.**

The key variables and parameters of this model of flagella mechanics are summarized in **Table S1** (which parallels **Table 1** in the main text).

Table S1. Key variables of the 1D PDE model of flagella mechanics

Variable	Definition (unit)
$\psi_n(s,t)$	Tangent angle of doublet n at location s and time t (rad)
$T_n(s,t)$	Tangential component of internal force in doublet n (pN)
$N_n(s,t)$	Normal component of internal force in doublet n (pN)
$M_{Bn}(s,t)$	Bending moment in doublet n (pN-μm)
$f_T(s,t)$	Inter-doublet tangential (shear) force per unit length (pN/μm)
$f_N(s,t)$	Inter-doublet normal force per unit length (pN/μm)
$q_{Tn}(s,t)$	Viscous tangential force per unit length (pN/μm)
$q_{Nn}(s,t)$	Viscous normal force per unit length (pN/μm)
$m(s,t)$	Net inter-doublet moment per unit length (pN)

The equilibrium equations for each doublet are:

	Doublet 1	Doublet 2	
$\boldsymbol{e}_T$:	$\frac{\partial T_1}{\partial s} - N_1\frac{\partial \psi_1}{\partial s} + f_T + q_{T1} = 0,$	$\frac{\partial T_2}{\partial s} - N_2\frac{\partial \psi_2}{\partial s} - f_T + q_{T2} = 0,$	(A.1ab)
$\boldsymbol{e}_N$:	$\frac{\partial N_1}{\partial s} + T_1\frac{\partial \psi_1}{\partial s} - f_N + q_{N1} = 0,$	$\frac{\partial N_2}{\partial s} + T_2\frac{\partial \psi_2}{\partial s} + f_N + q_{N2} = 0\,.$	(A.2ab)
ψ:	$\frac{\partial M_{B1}}{\partial s} + m + N_1 = 0,$	$\frac{\partial M_{B2}}{\partial s} + m + N_2 = 0.$	(A.3ab)

Each doublet is modeled as an elastic beam with flexural rigidity, EI:

$$M_{Bn} = EI\frac{\partial \psi_n}{\partial s}\,. \tag{A.4}$$

Using resistive force theory to model viscous drag, as in (2-4), the tangential and normal force components are:

$$q_{Tn} = -c_T v_{Tn}, \tag{A.5}$$

$$q_{Nn} = -c_N v_{Nn}. \tag{A.6}$$

where the velocity is $\boldsymbol{v}_n = v_{Nn}\boldsymbol{e}_{Nn} + v_{Tn}\boldsymbol{e}_{Tn}$. Using the kinematic relationships (2),

$$\frac{\partial v_T n}{\partial s} = v_N \frac{\partial \psi_n}{\partial s}, \tag{A.7}$$

$$\frac{\partial v_{Nn}}{\partial s} = \frac{\partial \psi_n}{\partial t} - v_T \frac{\partial \psi_n}{\partial s}, \tag{A.8}$$

the equilibrium, kinematic, and constitutive equations can be combined to form three equations for each doublet, describing the motion of a slender elastic beam moving in viscous fluid, subject to active and passive inter-doublet forces (2, 5).

$$T_{1,ss} - N_1\psi_{1,ss} - \left(1 + \frac{c_T}{c_N}\right) N_{1,s}\psi_{1,s} - \frac{c_T}{c_N} T_1 \psi_{1,s}^2 - \frac{c_T}{c_N} f_N \psi_{1,s} + f_{T,s} = 0, \tag{A.9a}$$

$$N_{1,ss} + \left(1 + \frac{c_N}{c_T}\right) T_{1,s}\psi_{1,s} + T_1\psi_{1,ss} - \frac{c_N}{c_T} N_1 \psi_{1,s}^2 + \frac{c_N}{c_T} f_T \psi_{1,s} + f_{N,s} = c_N \psi_{1,t}, \tag{A.9b}$$

$$EI\psi_{1,ss} + m + N_1 = 0. \tag{A.9c}$$

$$T_{2,ss} - N_2\psi_{2,ss} - \left(1 + \frac{c_T}{c_N}\right) N_{2,s}\psi_{2,s} - \frac{c_T}{c_N} T_2 \psi_{2,s}^2 + \frac{c_T}{c_N} f_N \psi_{2,s} - f_{T,s} = 0, \tag{A.9d}$$

$$N_{2,ss} + \left(1 + \frac{c_N}{c_T}\right) T_{2,s}\psi_{2,s} + T_2\psi_{2,ss} - \frac{c_N}{c_T} N_2 \psi_{1,s}^2 - \frac{c_N}{c_T} f_T \psi_{2,s} - f_{N,s} = c_N \psi_{2,t}, \tag{A.9e}$$

$$EI\psi_{2,ss} + m + N_2 = 0. \tag{A.9f}$$

Subscripts after the comma denote partial derivatives: $(.)_{,z} = \frac{\partial(.)}{\partial z}$. Parameters estimated for *Chlamydomonas* flagella (4, 6) (**Table 2**) are used, unless otherwise noted.

The following boundary conditions apply to the case in which each doublet is fixed at the base and free at its tip.

(A.9) (i) Zero angle at base: $\psi_n(0,t) = 0$

(A.9) (ii) Zero bending moment at distal end: $EI\psi_{n,s}(L,t) = 0$

(A.9) (iii) Zero transverse force at distal end: $N_n(L,t) = 0$

(A.9) (iv) Zero tangential force at distal end: $T_n(L,t) = 0$

(A.9) (v) Zero normal velocity at base 1 ($v_{N1}(0,t) = 0$): $\left[\frac{\partial N_1}{\partial s} + T_1 \frac{\partial \psi_1}{\partial s}\right]_{s=0} = -f_N$

(A.9) (vi) Zero tangent velocity at base 1 ($v_{T1}(0,t) = 0$): $\left[\frac{\partial T_1}{\partial s} - N_1 \frac{\partial \psi_1}{\partial s}\right]_{s=0} = -f_T$

(A.9) (vii) Zero normal velocity at base 2 ($v_{N2}(0,t) = 0$): $\left[\frac{\partial N_2}{\partial s} + T_2 \frac{\partial \psi_2}{\partial s}\right]_{s=0} = +f_N$

(A.9) (viii) Zero tangent velocity at base 2 ($v_{T2}(0,t) = 0$): $\left[\frac{\partial T_2}{\partial s} - N_2 \frac{\partial \psi_2}{\partial s}\right]_{s=0} = +f_T$

A.2 Inter-doublet forces due to steady, distributed dynein activity and passive components

Passive components of the axoneme resist doublet separation, coupling the motion of the two doublets. These components are modeled as distributed elements with linear elastic and viscous coefficients, k_N and b_N, respectively, and a nonlinear elastic coefficient k_{3N}.

$$\frac{\partial f_N}{\partial s} = -k_N(\psi_1 - \psi_2) - b_N\left(\psi_{1,t} - \psi_{2,t}\right) - k_{3N}(\psi_1 - \psi_2)^3. \quad \text{(A.10)}$$

In the tangential direction we include a *steady*, distributed dynein force per unit length, $f_T = pD(s)$, as well as passive resistance to inter-doublet sliding. The dynein distribution function, $D(s)$, allows the steady dynein activity to vary along the length. For longitudinally uniform dynein activity, $D(s) = 1$; for dynein activity that increases distally, $D(s) = 1 - \exp(s/s_0)$. The moments due to equal and opposite dynein forces on the P and R sides cancel (**Fig. S1**, **Fig. 3**), but the moments due to passive shear resistance add. The net inter-doublet moment per unit length is thus:

$$m = -k_T a^2 \bar{\psi} - b_T a^2 \bar{\psi}_{,t} - k_{3T} a^3 \bar{\psi}^3, \quad \text{(A.11)}$$

where the mean shear angle is $\bar{\psi} = (\psi_1 + \psi_2)/2$. The coefficients k_T and b_T represent linear elastic and viscous resistance to sliding (1, 7, 8), and k_{3T} a nonlinear stiffness. The nonlinear terms in Eqs. A.10-A.11 represent assumed nonlinear, stiffening behavior of elastic elements between doublets (3).

A.3 Linearized equation and boundary conditions

If both P and R sides of the flagellum are simultaneously active with identical baseline dynein activity, active bending moments will cancel. Accordingly, we study the stability of the zero (straight) equilibrium solution to Eqs. A.9 with dynein-driven tension and compression in the doublets, but only passive internal moments. To describe small-amplitude motion about a straight, equilibrium configuration, Eqs. A.9 may be linearized to obtain much simpler equations (5, 8, 9). Dropping terms that are nonlinear in the dependent variables, under uniform, steady dynein force ($D(s) = 1, f_T = p$), the baseline tension (or compression) in the two doublets is:

Doublet 1: $T_{10}(s) = p(L - s)$ (tension)

Doublet 2: $T_{20}(s) = -T_{10}$ (compression)

Equations A.9 then become

$$EI\psi_{1,ssss} - \frac{\partial}{\partial s}\left(p(L-s)\psi_{1,s}\right) + c_N\psi_{1,t} = -m_{,ss} - k_N(\psi_1 - \psi_2) - b_N\left(\psi_{1,t} - \psi_{2,t}\right) \quad \text{(A.12a)}$$

$$EI\psi_{2,ssss} + \frac{\partial}{\partial s}\left(p(L-s)\,\psi_{2,s}\right) + c_N\psi_{2,t} = -m_{,ss} + k_N(\psi_1 - \psi_2) + b_N\left(\psi_{1,t} - \psi_{2,t}\right) \quad \text{(A.12b)}$$

$$m = -k_T a^2 \bar{\psi} - b_T a^2 \bar{\psi}_{,t}. \qquad (\bar{\psi} = (\psi_1 + \psi_2)/2). \quad \text{(A.12c)}$$

Solutions to Eqs. A.12 must also satisfy appropriate boundary conditions. For example, if the flagellum is fixed at its proximal end ($s = 0$) and free at its distal end ($s = L$), solutions must satisfy the eight conditions:

(A.12) (i) Zero angle at base: $\psi_n(0,t) = 0, \quad n = 1,2$

(A.12) (ii) Zero moment at distal end: $EI\psi_{n,s}(L,t) = 0, \quad n = 1,2$

(A.12) (iii) Zero transverse force at distal end: $EI\psi_{n,ss}(L,t) + m(L,t) = 0, \quad n = 1,2$

(A.12) (iv) Zero normal velocity at base: $EI\psi_{1,sss}(0,t) + m_{,s}(0,t) = pL\psi_{1,s}$

(A.12) (v) Zero normal velocity at base: $EI\psi_{2,sss}(0,t) + m_{,s}(0,t) = -pL\psi_{2,s}$

A.4 Distally-increasing, steady, dynein force density

Other longitudinal distributions of dynein force will lead to slightly different PDEs and boundary conditions. For example, to model distally-increasing dynein activity, we use the function

$$D(s) = 1 - \exp(-s/s_0). \qquad \text{A.13}$$

To obtain the dynein shear force: $f_{TD} = pD(s)$. We use $s_0 = L/3$ in this study. Then the baseline tension in the doublets becomes:

Doublet 1: $T_{10}(s) = p\left[L + s_0 \exp\left(-\frac{L}{s_0}\right) - \left(s + s_0 \exp\left(-\frac{s}{s_0}\right)\right)\right]$ (tension)

Doublet 2: $T_{20}(s) = -T_{10}$, (compression).

In this case, the expression $p(L - s)$ in each of the equations of motion Eqs. A.12a-b is replaced by the corresponding baseline tension $T_{10}(s)$. The distribution functions and corresponding profiles of axial tension are shown in **Supplementary Fig. S3**.

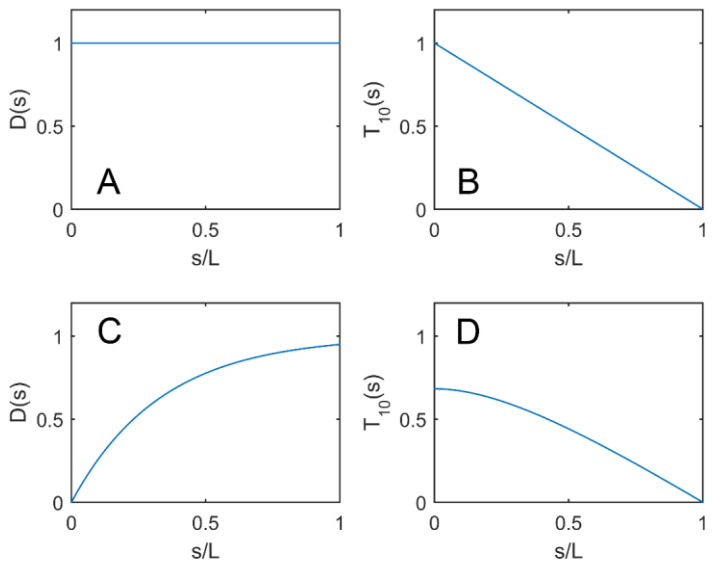

Supplementary Figure S3. Steady dynein force distributions and corresponding axial tension profiles. (**A**) *Uniform* distribution ($D(s) = 1$) of steady dynein force vs axial coordinate, s. (**B**) Baseline axial tension profile due to steady, uniform dynein activity. (**C**) *Distally-increasing* distribution $D(s) = 1 - e^{s/s_0}$ of steady dynein force vs axial coordinate, s, with $s_0 = L/3$. (**D**) Baseline axial tension profile due to steady, distally-increasing dynein activity.

B. STABILITY OF EQUILIBRIUM AND OSCILLATORY SOLUTIONS TO THE EQUATIONS OF MOTION

B.1 Definition of the eigenvalue problem

The behavior of the flagellum model can be described in terms of characteristic modes of oscillation, which are eigenfunctions of the linearized equations. Following references (5, 8, 10) and (1, 11), separable solutions are sought of the form

$$\psi_n(s,t) = \exp(\sigma t)\,\tilde{\psi}_n\,(s), \qquad n = 1{,}2 \tag{B.1}$$

with $\sigma = \alpha + i\omega$ (α and ω are real). Each such solution that satisfies the equation of motion and all boundary conditions is called an independent mode. If $\alpha > 0$, the mode grows exponentially. If M such modes are found with exponents σ_m and shape, $\tilde{\psi}_n^{(m)}(s)$, then a solution can also be formed from any linear combination of these modes: $\psi_n(s,t) = \sum_{m=1}^{M} a_m e^{\sigma_m t}\,\tilde{\psi}_n^{(m)}(s)$. In general, for arbitrary initial conditions, the least stable mode will dominate the response.

These separable solutions are substituted into the linearized equations of motion (Eqs. A.12). After defining a characteristic time for the system, $\tau = c_N L^4/EI$, and a normalized eigenvalue, $\bar{\sigma} = \sigma c_N L^4/EI$, the resulting ordinary differential equations (ODEs) may be written in non-dimensional form:

$$\tilde{\psi}_1'''' - \bar{p}\left[(1-\bar{s})\tilde{\psi}_1'\right]' + \bar{\sigma}\tilde{\psi}_1 = \bar{c}(\bar{\sigma})(\tilde{\psi}_1'' + \tilde{\psi}_2'') - \bar{d}(\bar{\sigma})(\tilde{\psi}_1 - \tilde{\psi}_2), \quad \text{(B.2a)}$$

$$\tilde{\psi}_2'''' + \bar{p}\left[(1-\bar{s})\tilde{\psi}_2'\right]' + \bar{\sigma}\tilde{\psi}_2 = \bar{c}(\bar{\sigma})(\tilde{\psi}_1'' + \tilde{\psi}_2'') + \bar{d}(\bar{\sigma})(\tilde{\psi}_1 - \tilde{\psi}_2), \quad \text{(B.2b)}$$

where the new non-dimensional parameters are $\bar{p} = pL^3/EI$, $\bar{c}(\bar{\sigma}) = (k_T a^2 + b_T a^2\,\bar{\sigma})L^2/EI$, and $\bar{d}(\bar{\sigma}) = (k_N + b_N\,\bar{\sigma})L^2/EI$.

(B.2) (i)	Zero angle at base:	$\tilde{\psi}_n(0) = 0, \quad n = 1,2$
(B.2) (ii)	Zero moment at distal end:	$\tilde{\psi}_n'(1) = 0, \quad n = 1,2$
(B.2) (iii)	Zero transverse force at distal end:	$\tilde{\psi}_n''(1) - \bar{c}(\bar{\sigma})(\tilde{\psi}_1 + \tilde{\psi}_2) = 0, \quad n = 1,2$
(B.2) (iv)	Zero normal velocity at base:	$\tilde{\psi}_1'''(0) - \bar{c}(\bar{\sigma})(\tilde{\psi}_1' + \tilde{\psi}_2') = \bar{p}\tilde{\psi}_1'$
(B.2) (v)	Zero normal velocity at base:	$\tilde{\psi}_2'''(0) - \bar{c}(\bar{\sigma})(\tilde{\psi}_1' + \tilde{\psi}_2') = -\bar{p}\tilde{\psi}_2'$

These two coupled ODEs, together with the associated boundary conditions, form an eigenvalue problem. The coupling between these two differential equations, as well as the factor of $1 - \bar{s}$ complicate the solution of the eigenvalue problem, so that numerical methods (weighted residual or finite element calculations, e.g.) are required to find the natural modes and frequencies of oscillation.

Approximate solutions to the eigenvalue problem can be obtained using numerical methods. Such methods include finite element analysis and the method of weighted residuals (12). Eigenfunctions can be approximated by linear combinations of the vibration modes of an Euler-Bernouilli beam with fixed-free boundary conditions. The application of the method of weighted residuals to this problem is described in reference (11) and in section B.2 below.

B.2 Solution of eigenvalue problem by the method of weighted residuals

The eigenvalue problem was solved numerically by the method of weighted residuals (12) with up to $N = 12$ trial functions to obtain a matrix form of the eigenvalue problem.

We can approximate $\tilde{\psi}$ by a linear combination of admissible functions (12):

$$\tilde{\psi}_1(\bar{s}) \approx \sum_{j=1}^{N} q_{1j} Q_j(\bar{s}), \qquad \tilde{\psi}_2(\bar{s}) \approx \sum_{j=1}^{N} q_{2j} Q_j(\bar{s}) \quad \text{(B.3)}$$

These expressions are substituted into the eigenfunction equations and boundary conditions, and the residual error weighted by each of a set of test functions, $\phi_i(\bar{s})$ and weighting factors $w_i^{(k)}$ is set to zero. In this method the weighting factor for the $s = 0$ boundary condition is $w_i^{(0)} = \phi_i(0)$ and at the opposite end ($s = 1$), $w_i^{(1)} = \phi_i'(1)$. For the case of uniform dynein activity, we obtain:

$$\sum_{j=1}^{N} q_{1j}\left\{\int_0^1 \phi_i\, Q_j''''\, d\bar{s} - \int_0^1 \phi_i \bar{p}\left[(1-\bar{s})Q_j'\right]' d\bar{s} + \bar{\sigma}\int_0^1 \phi_i Q_j\, d\bar{s} - \bar{c}(\bar{\sigma})\int_0^1 \phi_i Q_j''\, d\bar{s} + \bar{d}(\bar{\sigma})\int_0^1 \phi_i Q_j\, d\bar{s} + w_i^{(1)}\left[Q_j''(1) - \bar{c}(\bar{\sigma})Q_j(1)\right] + w_i^{(0)}\left[Q_j'''(0) - \bar{c}(Q_j'(0) - \bar{p}Q_j'(0)\right]\right\} + \sum_{j=1}^{N} q_{2j}\left\{-\bar{c}(\bar{\sigma})\int_0^1 \phi_i Q_j''\, d\bar{s} - \bar{d}(\bar{\sigma})\int_0^1 \phi_i Q_j\, d\bar{s} - w_i^{(1)}\left[\bar{c}(\bar{\sigma})Q_j(1)\right] - w_i^{(0)}\left[\bar{c}(\bar{\sigma})Q_j'(0)\right]\right\} = 0, \quad \text{(B.4a)}$$

$$\sum_{j=1}^{N} q_{2j}\left\{\int_0^1 \phi_i\, Q_j''''\, d\bar{s} + \int_0^1 \phi_i \bar{p}\left[(1-\bar{s})Q_j'\right]' d\bar{s} \;+\; \bar{\sigma}\int_0^1 \phi_i Q_j\, d\bar{s} - \bar{c}(\bar{\sigma})\int_0^1 \phi_i Q_j''\, d\bar{s} - \bar{d}(\bar{\sigma})\int_0^1 \phi_i Q_j\, d\bar{s} + w_i^{(1)}\left[Q_j''(1) - \bar{c}(\bar{\sigma})Q_j(1)\right] + w_i^{(0)}\left[Q_j'''(0) - \bar{c}(Q_j'(0) + \bar{p}Q_j'(0)\right]\right\} + \sum_{j=1}^{N} q_{1j}\left\{-\bar{c}(\bar{\sigma})\int_0^1 \phi_i Q_j''\, d\bar{s} + \bar{d}(\bar{\sigma})\int_0^1 \phi_i Q_j\, d\bar{s} - w_i^{(1)}\left[\bar{c}(\bar{\sigma})Q_j(1)\right] - w_i^{(0)}\left[\bar{c}(\bar{\sigma})Q_j'(0)\right]\right\} = 0. \tag{B4b}$$

Analogous equations can be obtained for other dynein distributions. The $2N$ equations for the weighted residual error may be integrated by parts, simplified and expressed as matrix-vector system:

$$\left[K^{(11)} + \bar{\sigma}C^{(11)}\right]\boldsymbol{q_1} + \left[K^{(12)} + \bar{\sigma}C^{(12)}\right]\boldsymbol{q_2} = \mathbf{0}, \tag{B.5a}$$

$$\left[K^{(21)} + \bar{\sigma}C^{(21)}\right]\boldsymbol{q_1} + \left[K^{(22)} + \bar{\sigma}C^{(22)}\right]\boldsymbol{q_2} = \mathbf{0}, \tag{B.5b}$$

Where the $N \times N$ matrices K and C contain the coefficients of q_j in the i^{th} equation above. Defining

$$\boldsymbol{q} = \begin{bmatrix}\boldsymbol{q_1}\\ \boldsymbol{q_2}\end{bmatrix}, \tag{B.6}$$

we obtain the compact form of the eigenvalue problem:

$$[K + \bar{\sigma}C]\boldsymbol{q} = \mathbf{0} \tag{B.7}$$

$$K = \begin{bmatrix}K^{(11)} & K^{(12)}\\ K^{(21)} & K^{(22)}\end{bmatrix}, \quad C = \begin{bmatrix}C^{(11)} & C^{(12)}\\ C^{(21)} & C^{(22)}\end{bmatrix} \tag{B.8}$$

The matrix elements were calculated numerically using numerical quadrature, and the resulting matrix eigenvalue problem was solved using MATLAB software (The Mathworks, Natick, MA). The free vibration modes of a uniform, fixed-free beam were used as trial functions (Q_j) for flagella with fixed-free boundary conditions.

C. ADDITIONAL RESULTS

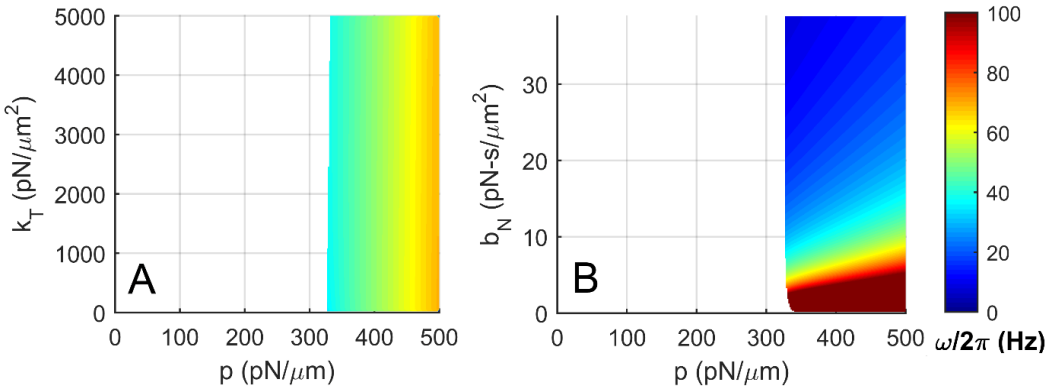

Supplementary Figure S4. Oscillatory behavior of the 1D PDE model (two-doublet system) with steady, uniform, dynein loading obtained by eigenanalysis of the linearized PDEs. (**A**) Oscillation frequency vs shear stiffness k_T, and dynein force density, p, for conditions in which the straight equilibrium configuration is unstable. (**B**) Oscillation frequency vs coupling viscous resistance, b_N, and dynein force density, p. Other parameters are given in **Table 2**.

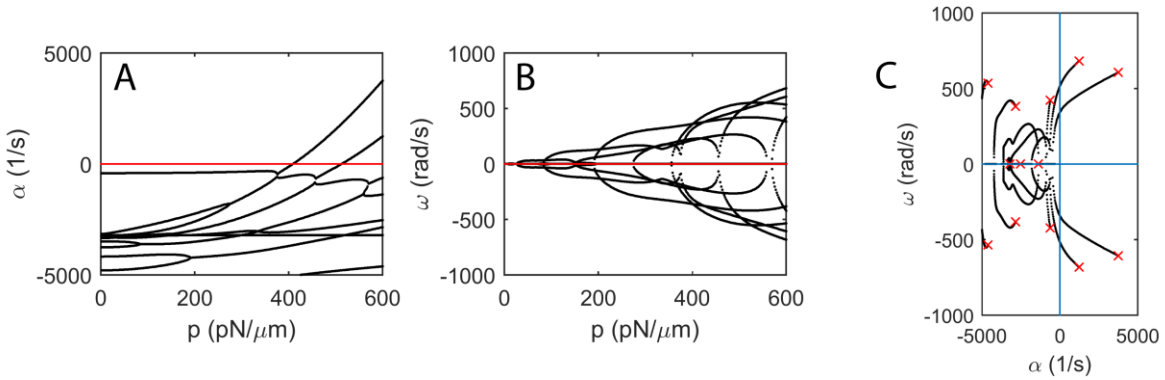

Supplementary Figure S5. Stability analysis of the 1D PDE model (two-doublet system) with steady, distally-increasing, dynein loading of amplitude p (pN/µm). (**A**) Real and (**B**) imaginary parts of eigenvalue of the linearized equations as the amplitude of the steady dynein load is increased. A dynamic instability occurs near p =410 pN/µm when the real parts of one pair of eigenvalues become positive while the imaginary parts are non-zero. (**C**) Root locus showing the trajectories of the eigenvalues from the left (stable) to right (unstable) half-plane, as p increases.

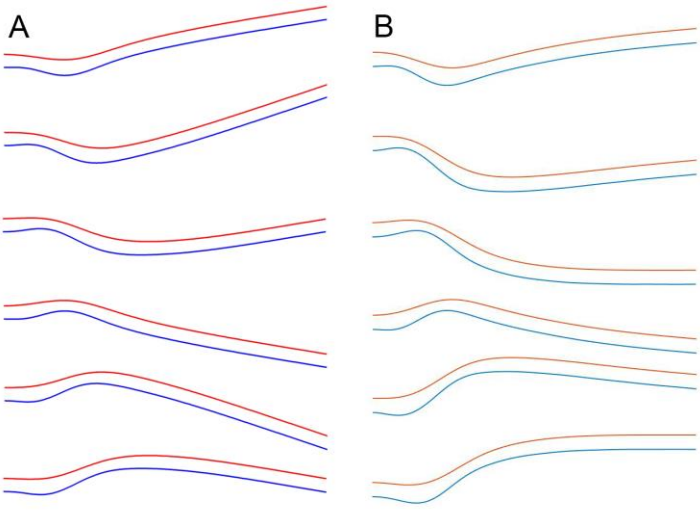

Figure S6. Predicted shapes of both doublets in the 1D PDE model (two-doublet system) at six equally-spaced intervals during the flagellar beat. Flutter instability and flagellar oscillations are induced by steady, uniformly-distributed dynein loading with force density p=350 pN/μm. (**A**) The first mode of the linearized system. (**B**) Shape predicted by simulation of the nonlinear PDEs (motion will include contributions from more than one mode).

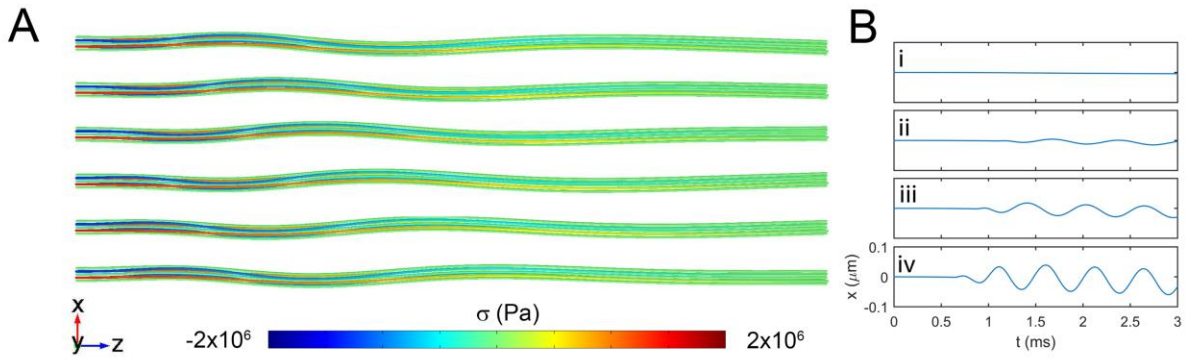

Supplementary Figure S7. (**A**) Snapshots from the time-domain simulation of the 3D FE model of the flagellum (six doublets) with length L=12 μm, total flexural rigidity EI_f=700 pN-μm^2, under steady, *uniformly-distributed* dynein loading of amplitude p=174 pN/μm per active doublet. Images are shown at six equally-spaced phases during one period of oscillation (A) Side-view ($X-Z$ plane). Color indicates axial stress along the centerline: red (positive) = tension; blue (negative) = compression. (**B**) Tip position vs time in simulations of the 3D FE structural model of the flagellum with steady, uniformly-distributed dynein loading, p. (i) p =46 pN/μm. (ii) p =69 pN/μm. (ii) p =93 pN/μm. (iv) p =116 pN/μm. Above a critical value of dynein force density, p, the straight equilibrium configuration becomes unstable, and a limit cycle emerges.

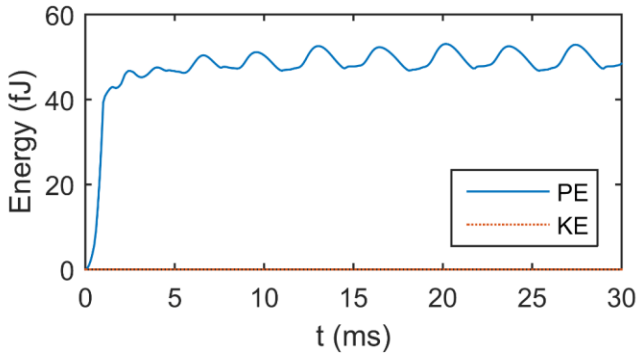

Supplementary Figure S8. Time series of potential energy and kinetic energy during oscillations of the 3D finite element model of the axoneme. The kinetic energy is negligible, even after mass scaling, confirming that inertial effects are not significant.

D. SUPPLEMENTARY MOVIE LIST

Movie M1: Flutter of beam with a constant-amplitude, tangential (follower) tip load (**Fig. 2C**). The non-dimensional load amplitude is $\bar{P} = PL^2/EI = 48$.

Movie M2: Oscillatory wave-like motion of two coupled doublets predicted by stability analysis of the 1D PDE model; the movie shows the least stable mode (eigenfunction) of the linearized equations with steady, uniform dynein density amplitude p=350 pN/μm (see **Fig. 4A**).

Movie M3: Waveform predicted by time-domain simulation of the nonlinear equations of motion of the 1D PDE model with distally-increasing dynein density amplitude p=450 pN/μm.

Movie M4: Waveform predicted by time-domain simulation of the nonlinear equations of motion of the 1D PDE model with distally-increasing dynein density amplitude p=600 pN/μm (**Fig. 5C**).

Movie M5: Waveform predicted by time-domain simulation of the nonlinear equations of motion of the 1D PDE model with distally-increasing dynein density amplitude p=800 pN/μm (**Fig. 5D**).

Movie M6: Oscillatory motion predicted by time-domain simulation of a 3D FE structural model of an axoneme with simultaneous antagonistic dynein activity on opposing doublets with distally-increasing, dynein force amplitude p=184 pN/μm (**Fig. 6**). Viewed in the $X - Z$ plane.

Movie M7: Oscillatory motion predicted by simulation of the 3D FE model of the axoneme with distally-increasing, dynein force amplitude p=184 pN/μm (**Fig. 6**). Viewed in the $X - Y$ plane.

REFERENCES - SUPPLEMENT

1. Bayly PV & Wilson KS (2014) Equations of inter-doublet separation during flagella motion reveal mechanisms of wave propagation and instability *Biophys J* 107(7):1756-1772.
2. Hines M & Blum JJ (1978) Bend propagation in flagella. I. Derivation of equations of motion and their simulation. *Biophys J* 23(1):41-57.
3. Brokaw CJ (1972) Computer simulation of flagellar movement. I. Demonstration of stable bend propagation and bend initiation by the sliding filament model. *Biophys J* 12(5):564-586.
4. Bayly PV*, et al.* (2011) Propulsive forces on the flagellum during locomotion of Chlamydomonas reinhardtii. *Biophys J* 100(11):2716-2725.
5. Hilfinger A, Chattopadhyay AK, & Julicher F (2009) Nonlinear dynamics of cilia and flagella. *Phys Rev E Stat Nonlin Soft Matter Phys* 79(5 Pt 1):051918.
6. Xu G*, et al.* (2016) Flexural Rigidity and Shear Stiffness of Flagella Estimated from Induced Bends and Counterbends. *Biophysical Journal* In press.
7. Bayly PV, Lewis BL, Kemp PS, Pless RB, & Dutcher SK (2010) Efficient spatiotemporal analysis of the flagellar waveform of Chlamydomonas reinhardtii. *Cytoskeleton (Hoboken)* 67(1):56-69.
8. Riedel-Kruse IH, Hilfinger A, Howard J, & Julicher F (2007) How molecular motors shape the flagellar beat. *HFSP J* 1(3):192-208.
9. Fu HC, Wolgemuth CW, & Powers TR (2008) Beating patterns of filaments in viscoelastic fluids. *Phys Rev E* 78(4).
10. Camalet S & Julicher F (2000) Generic aspects of axonemal beating. *New J Phys* 2:241-2423.
11. Bayly PV & Wilson KS (2015) Analysis of unstable modes distinguishes mathematical models of flagellar motion. *Journal of the Royal Society, Interface / the Royal Society* 12(106).
12. Meirovitch L (1997) *Principles and techniques of vibrations* (Prentice Hall, Upper Saddle River, N.J.) pp x, 694 p.